frontiers | Frontiers in Earth Science

ORIGINAL RESEARCH
published: 17 June 2022
doi: 10.3389/feart.2022.879387

Stability Control of Slopes in Open-Pit Mines and Resilience Methods for Disaster Prevention in Urban Areas: A Case Study of Fushun West Open Pit Mine

Zhou Jiaxing[1], *Li Fei*[1]*, *Wang Jin-an*[1,2], *Gao Anqi*[3] *and He Chengyuan*[4,5]

[1]School of Civil and Resource Engineering, University of Science and Technology Beijing, Beijing, China, [2]State Key Lab of Education Ministry for High Efficient Mining and Safety of Metal Mine, University of Science and Technology Beijing, Beijing, China, [3]Shanxi Academy of Building Research Co., Ltd., Taiyuan, China, [4]China Railway Bridge Research Institute, Ltd., Wuhan, China, [5]State Key Laboratory for Health and Safety of Bridge Structure, Wuhan, China

OPEN ACCESS

Edited by:
Bo Li,
Tongji University, China

Reviewed by:
Haiping Yuan,
Hefei University of Technology, China
Lei Wang,
ANHUI.HUAINAN, China
Kang Zhao,
Jiangxi University of Science and Technology, China

***Correspondence:**
Li Fei
lifei3522883@163.com

Specialty section:
This article was submitted to Geoscience and Society, a section of the journal Frontiers in Earth Science

Received: 19 February 2022
Accepted: 11 May 2022
Published: 17 June 2022

Citation:
Jiaxing Z, Fei L, Jin-an W, Anqi G and Chengyuan H (2022) Stability Control of Slopes in Open-Pit Mines and Resilience Methods for Disaster Prevention in Urban Areas: A Case Study of Fushun West Open Pit Mine. Front. Earth Sci. 10:879387. doi: 10.3389/feart.2022.879387

During the century-long mining process of the Fushun west open pit, slope slippage and deformation caused varying degrees of horizontal deformation, uneven settlement, and ground cracks on the surface of the urban areas, which caused a certain degree of damage to buildings and infrastructure and affected the livings of residents in the surrounding communities. In this study, a set of building reinforcement and community resilience enhancement methods that can resist slope deformation was proposed to improve the ability of urban areas to cope with slope geological hazards and emergency response. The main research contents included: Firstly, this paper systematically analyzed the deformation mechanism of the dip sloping and the inverse dip sloping section of the open pit mine, which was based on the field measured data and simulation calculation results. In other words, the horizontal deformation of the stratum in the dip sloping section was dominant, while the stratum in the inverse dip sloping section was prone to ground cracks and uneven settlement. In view of this, three surface deformation characteristic subdivisions of the surrounding urban area were proposed. In addition, a study on the damage characteristics of buildings with different types of foundations and structures under the influence of side slope deformation were carried out, and the anti-deformation reinforcement measures for load-bearing members mainly based on steel fiber concrete, carbon fiber materials and profile steel were proposed. Finally, a three-level disaster emergency setting system for urban areas around open pit mine was established, and the disaster prevention and resilience enhancement strategy for build and unbuilt the communities around the side slopes was constructed. The study aims to provide technical support to the overall resilience and response of the urban communities adjacent to open-pit mine slopes against consequent geological hazards and emergencies, thereby promoting sustainable urban development.

Keywords: open pit slope, solpe deformation, deformation-resistant reinforcement, disaster resilience, building damage

INTRODUCTION

The Fushun western open pit has a 100-years mining history and has now formed a deep and large pit with an east-west length, north-south width, and depth of 6.6 km, 2 km and 400 m, respectively, disturbing over an area of 15 km^2. Since the mining of the western open pit and the development and construction of the city were in the same period of history, the city of Fushun has formed a complex urban spatial layout with "a mine in the city and a city on the mine." The engineering geology and hydrogeological conditions of the western open-pit mine area are exceptionally intricate, and there are various environmental and geological hazards such as water pollution, landslides, and ground cracks, which have caused different degrees of damage and impact on the urban buildings and infrastructure around the western open-pit mine, thus causing serious impacts on the safety of urban residential areas.

In recent years, a number of studies have been carried out on the building resistance against slope deformation and geological hazards in urban areas (Du et al., 2020). In terms of landslide prevention and emergency response, Du et al. (2021) analyzed the mechanism of slope rock collapse disaster genesis, developed high-precision remote sensing vibration monitoring and early warning technology, and established monitoring and early warning protocols with bedrock separation damage precursors as the core. Chen et al. (2015) established a real-time, effective, and intelligent geological disaster prevention and control management system, which realized disaster information management, real-time monitoring, forecasting and warning of geological disasters, and emergency evacuation of the public. Ou et al. (2021) based 14 geo-environmental factors such as slope, elevation, fault, rainfall, and lithology, and used the binary logistic regression model (LRM) to evaluate the landslide hazard, in order to provide technical support for disaster mitigation and prevention in Jiangxi province. Xu et al. (2020) established a geological disaster prevention strategy that combines disaster risk management with disaster mitigation, sustainable livelihoods, and poverty alleviation, thereby improving the community's resilience to landslide hazards. Tsai et al. (2021) investigates water saturation changes over time using time-lapse Electrical Resistivity Tomography (ERT) images, providing a powerful method for monitoring landslide events. Shao (2019) analyzed the characteristics of geological hazards in mines caused by high-intensity mining, established a database of hazards, and proposed measures to enhance landslide hazard prevention and control. La et al. (2021) based on the "disaster scenario—rescue task—rescue object—demand prediction—object deployment," the NSGA-II algorithm for the rescue object deployment model was established using a data of 18 representative slope disaster rescue operations in the past, so as provide effective guidelines for the rescue work. Moreover, the deep displacement-based monitoring method is of great significance to the investigation of early warning indicators and deformation monitoring of natural landslides, to reduce/avoiding the consequences caused by landslides (Chen et al., 2021). Aiming at the mechanism of rainfall-induced landslides and the mechanism of rainfall impact on slopes, a set of Spatio-temporal monitoring and early warning system of landslides based on multi-scale Spatio-temporal analysis and remote sensing technology was established to provide a basis for the prevention of disasters (He et al., 2022). Regarding the deformation resistance of buildings, an improved high-performance polymer cement mortar (PCM) and glass fiber reinforced plastic (GFRP) composites were used by (Qiao et al., 2022) to strengthen and repair masonry structures. Mostafa et al. (2021) proposed glass fiber reinforced concrete beams containing transverse reinforcement, which effectively enhanced the buckling resistance of beams under service and ultimate loads. Gulec et al. (2021) used prefabricated cages to strengthen T-section concrete beams, which show better flexural and ductile properties than conventional reinforcement methods. Rf et al. (2020) investigated a reinforcement solution for concrete floor slabs having a higher top reinforcement near the column, which significantly increased the impact resistance and reduced the flexural deflection. Resan et al. (2020) proposed a composite beam structure with embedded steel plates in shear span based on the results of the four-point load limit damage test, which effectively improved the stiffness and strength of the structure.

However, the available literature only covers two basic aspects of disaster prevention and control or emergency response and does not provide systematic guidelines to enhance the disaster prevention and resilience of buildings and residents in areas affected by geological hazards. To aims to effectively improve the disaster resilience and sustainable urban development of the residential communities in the impact area, this study systematically analyzed the damage characteristics of buildings and surfaces in urban areas, and proposed a deformation-resistant reinforcement scheme for buildings and an optimized strategy for communities disaster prevention and mitigation in the Fushun west open-pit mine impact zone.

SURFACE DEFORMATION ZONING IN URBAN AREAS AROUND THE SLOPES OF OPEN PIT MINES

Surface Monitoring and Characterization of Urban Areas

Figure 1 shows the trend of surface displacement variables in the Fushun west open-pit mine and the surrounding urban area from 2016 to 2020. Relevant data derived from the Interferometric Synthetic Aperture Radar on Board technology (InSAR) monitoring the regional surface. The areas with large surface deformation in the city are the Qian-tai mountain area in the south bank (within the former landslide body), the central and western part of the north bank (former petroleum plant No. 1), the eastern part of the north bank and the western drainage field. In the area of the discharge site on the west bank, the vertical displacement of the surface has increased significantly due to the continuous accumulation and settlement of the discharge. The surface deformation in this area is independent of the pit slope deformation and engineering disturbance, and its no impact on the surface deformation in the urban area.

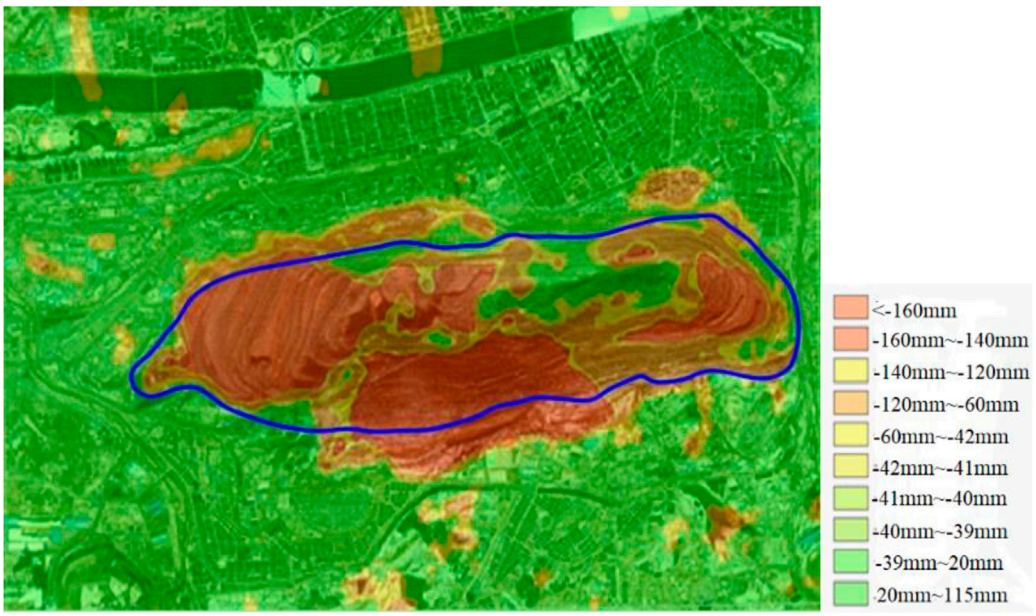

FIGURE 1 | Cumulative surface displacement map of west open pit and affected area from 2016 to 2020.

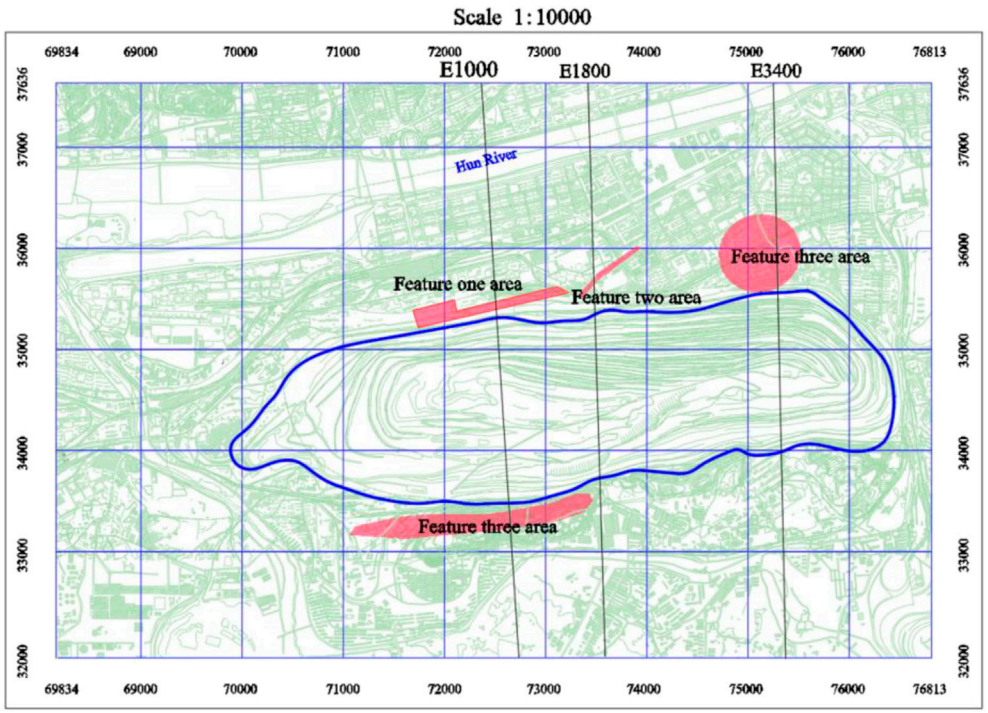

FIGURE 2 | Deformation zone map of the west open-pit influence area.

The central part of the northern bank is dominated by vertical deformation of the ground surface under the influence of ground fracture and slope creep deformation. Surface deformation in the area of ground cracks in the east-central part of the northern bank is subjugated by uneven settlement and horizontal deformation. The area of Qian-tai mountain on the south bank falls within the original landslide zone. In recent years, with the implementation of backfill and other slope management projects, the vertical deformation of the stratum has been reduced; consequently, the horizontal deformation of the ground surface is dominant. The

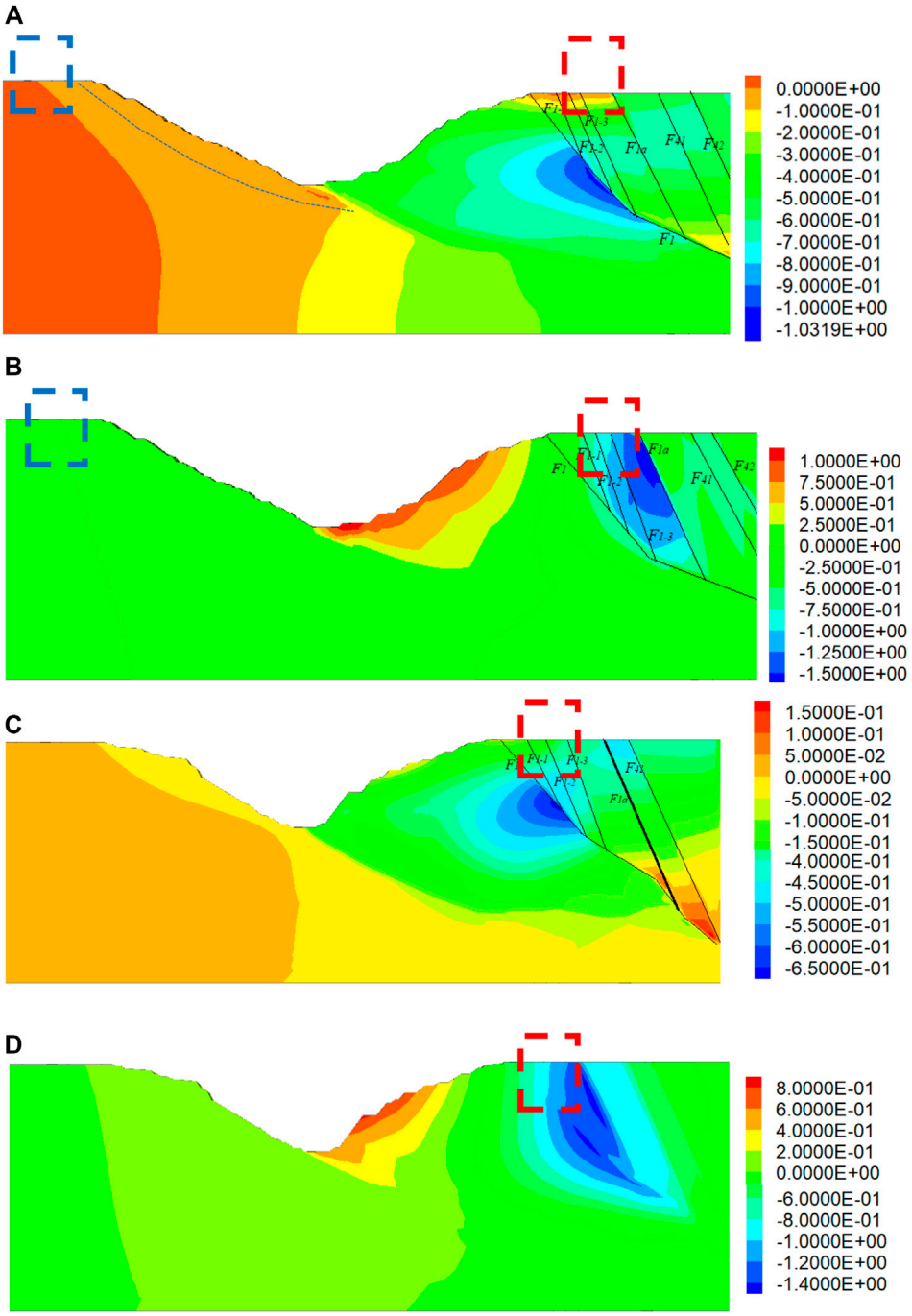

FIGURE 3 | (Continued).

eastern area of the north bank is adjacent to the F_1 fault, the overall stability of the strata is reduced, and the horizontal deformation of the ground surface has increased. In this study, the four areas with large surface displacements monitored on-site were divided into three deformation characteristic zones as shown in **Figure 2** (Gao et al., 2021) based on the actual field survey and relevant literature.

Calculation and Analysis of Slopes Deformation Trends

To analyze the deformation characteristics of the strata affected by previous excavation disturbance in each part of the urban area and to reveal the induced mechanism of surface deformation in each area, FLAC3D numerical simulation software was used. A two-dimensional model was prepared for computation, in which

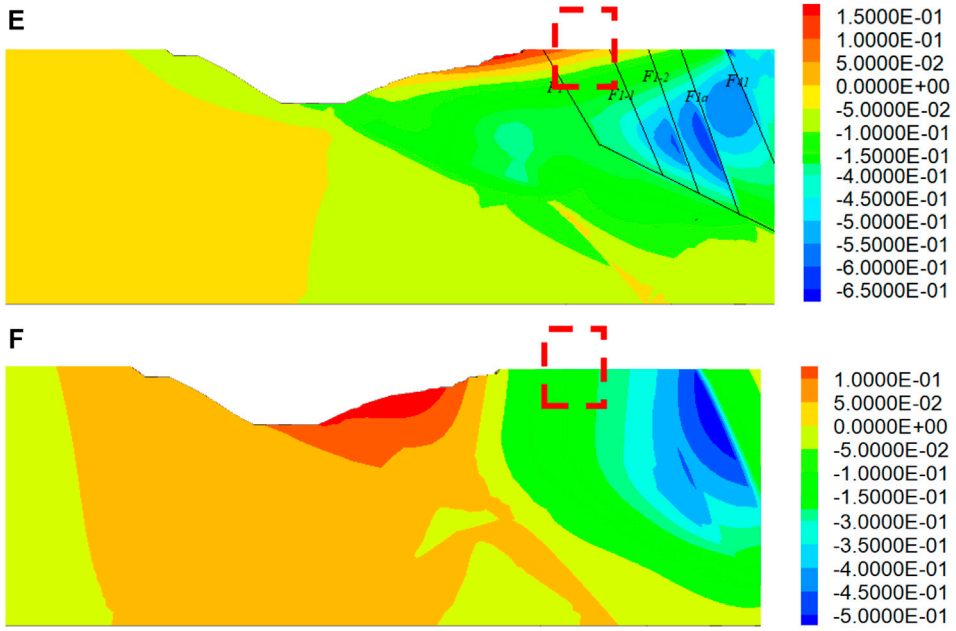

FIGURE 3 | (Continued). Distribution of stratigraphic displacements in each feature zone: **(A)** stratigraphic horizontal displacement of the E1000 profile in feature-1; **(B)** vertical displacement of strata of the E1000 profile in feature-1; **(C)** stratigraphic horizontal displacement of the E1800 profile in feature-2; **(D)** vertical displacement of strata of the E1800 profile in feature-2. **(E)** stratigraphic horizontal displacement of the E3400 profile in feature-3; **(F)** vertical displacement of strata of the E3400 profile in feature-3.

the width of the fault was defined in accordance with the actual width, and the mechanical parameters of the fault units was discount. The material parameters and excavation timing of the computation model were in line with (Gao, 2020). The slope excavations from 1950 to the hitherto were analyzed for the E1000, E1800 E3400 profiles involved in deformation feature-1, feature-2, and feature-3, respectively. The displacement field distribution of each profile is shown in **Figure 3**.

Figure 3A,B shows the distribution of slope and surface deformation in the E1000 section of the west open-pit slope, wherein the stratigraphic range of feature-1 is highlighted by the red box, and the stratigraphic range of the Qian-tai mountain area is highlighted by the blue box. The horizontal deformation of the stratum mainly occurred at the F_1 fault structure in the north bank area due to the effect of the slope excavation disturbance since 1950. It was observed that the amount of horizontal ground displacement within the feature-1 area was large, and the value of the variation of displacement in the area was about 400 mm. The area having maximum vertical deformation in the strata was the neighboring area of $F_{1\text{-}1}$, $F_{1\text{-}2}$, and $F_{1\text{-}3}$ faults, and the accumulated surface deformation was about 1500 mm. The area of maximum deformation was located within the feature-1 area. The amount of variation of horizontal displacement of the surface in the area of the Qian-tai mountain was large; meanwhile, the variation of vertical displacement was relatively small.

Figure 3C,D shows the distribution of slope and surface deformation in the E1800 profile, wherein the surface area of feature-2 is indicated in the red box. The horizontal deformation of the north bank stratum mainly occurred in the same level section between the F_1 fault and the bottom of the pit. The accumulated maximum deformation was about 650 mm, and the maximum horizontal deformation of the ground surface was relatively small. The maximum vertical deformation area of the stratum was involved $F_{1\text{-}1}$, $F_{1\text{-}2}$, and $F_{1\text{-}3}$ faults, and the accumulated deformation of the surface was about 1400 mm, which was less than the feature-1 zone. The surface deformation of the south bank was small, and the stability of the stratum was relatively high.

Figure 3E,F shows the distribution of slope and surface deformation in the E3400 profile of the west open-pit mine, wherein the red box shows the surface area of feature-3. The stratigraphic stability of the north bank was observed to be relatively stable, and the surface deformation was small. The horizontal displacement of the stratum in the north bank is large in the feature-3 area, with a peak of around 200 mm. Meanwhile, the differential settlement deformation was relatively small in this area.

Slope Deformation-Induced Mechanisms

(1) Feature-1 Area: both horizontal and vertical displacements were relatively large

Feature-1 area is the area near the former petroleum plant on the north bank, and the regional stratigraphy is formed by sandstone wedge bodies bounded by the F_1 fault and the F_{1A} fault, as shown in **Figure 4A**. Due to the low strength and hardness of the rock formation, the wedge (red filled area) was affected by the coupled effect of the lateral pressure of the hard granite stress field on the east side and the unloading force on the surface near the side slope body on the west side. This resulted in

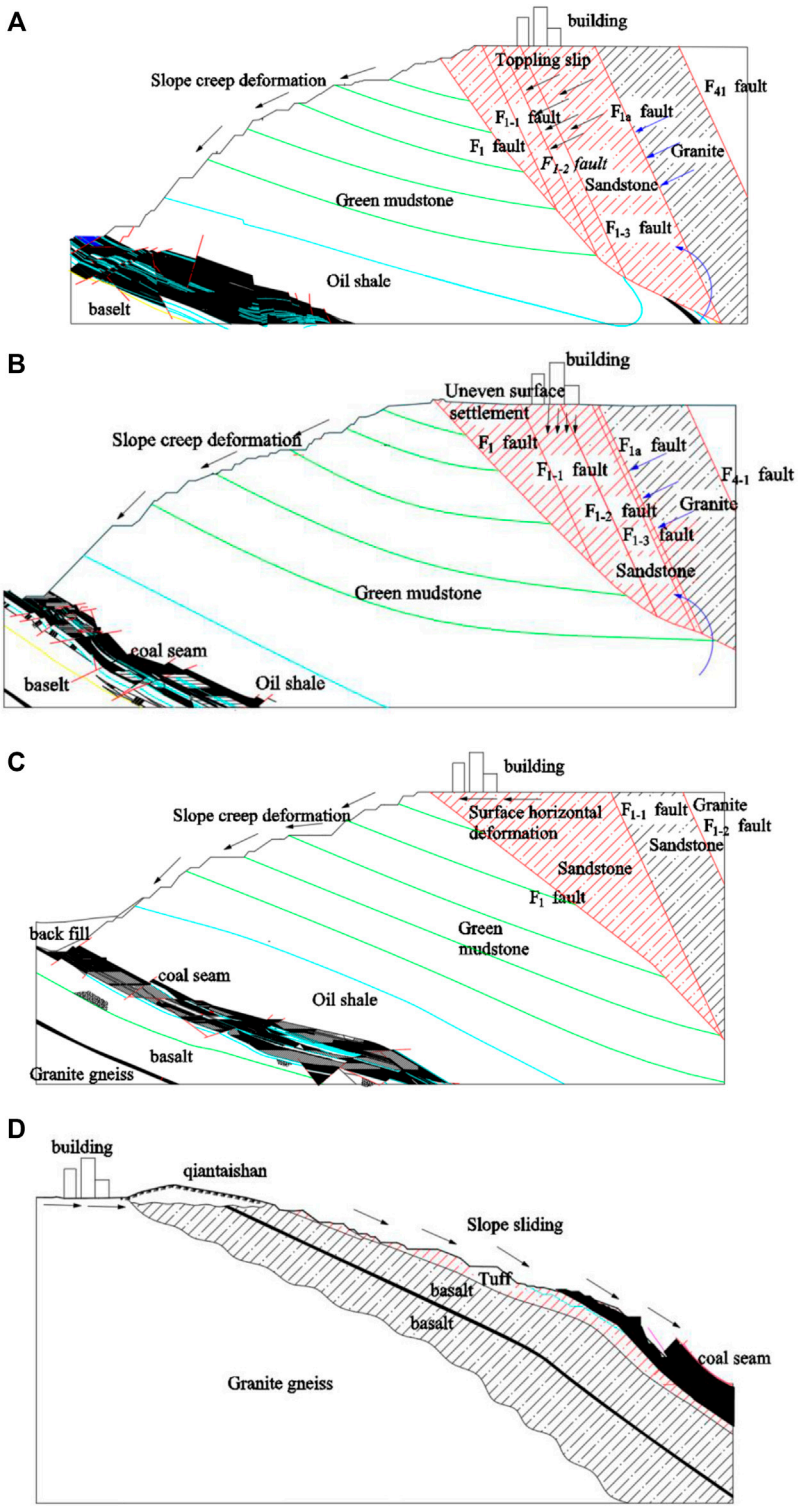

FIGURE 4 | Sliding deformation mechanism of slopes in each feature zone: **(A)** feature-1 Zone Wedge Rotating Slip; **(B)** feature-2 Zone Wedge Dumping Slip; **(C)** feature-3 zone Wedge Flush Slip; **(D)** feature-3 area south gang slope body downward sliding.

an overall rotational slip at the intersection of the two faults, which caused a large horizontal and vertical ground surface displacement. Owing to this, the surface deformation in the central part of the northern bank was mainly influenced by two geological feature-s, i.e., 1) the adjacent slope body, which undergoes creep deformation and results in an increased

horizontal deformation of the ground surface; 2) the large faults across the region, which induce misalignment of ground fracture zone and cause uneven ground settlement. Moreover, this area is adjacent to the slope having a landslide history in 2016 due to the heavy rainfall; thus, the foundation and bottom wall of the building (structure) in this area are prone to failure, i.e., cracking and shedding.

(2) Feature-2 area: vertical displacement was relatively large

Feature-2 area is the junction region of roads, i.e., Xi'san Street, Jie'fang Road, and Xi'qi Road in the east-central part of the north bank, which is the majorly affected area by the ground fracture misalignment induced by the activation of the F_{1a} fault. As shown in **Figure 4B**, a layer of fault fracture zone exists between the east side of the wedge and the granite area, which decreases the lateral pressure from the east side. The distance of the west side of the wedge from the slope increases, leading to a decrease in the unloading force by the slope. The wedge geologic body undergoes dumping slip and induces fault activation in the upper part of the wedge. Therefore, the area is dominated by vertical deformation, buildings and roads are prone to failure, i.e., cracking and tumbling.

(3) Feature-3 area: horizontal displacement was relatively large

The south of Nan'yang Road is located at the eastern surface of the north bank wedge, and there is no large fracture structure inside the wedge geological body in this area. Its overall stiffness is relatively high, and its east side is subjected to weaker thrusts from the geological body composed of granite. As shown in **Figure 4C**, the F_1 fault is close to the slope surface, the overall stability of this stratum is low. The wedge-shaped geological body is prone to translating and triggering a large horizontal deformation of the ground surface. Also, the horizontal deformation of the ground surface is induced by the influence of creep deformation of the slope. The foundations of the buildings are susceptible to shear damage, due to which the superstructure can be separated from the foundation by cracking.

The Qian-tai mountain area has a landslide history. As shown in **Figure 4D**, the surface deformation is relatively large due to the influence of adverse geological conditions, i.e., two sets of large fracture zones and down-sloping slopes. In recent years, with the implementation of slope management projects such as backfilling, the vertical deformation of the stratum has been reduced. The surface deformation in the area is mainly horizontal, and the exterior walls of the buildings are prone to cracking.

ANALYSIS OF DETERIORATION CHARACTERISTICS AND DEFORMATION RESISTANCE OF BUILDINGS AROUND SLOPES

In order to analyze of deformation damage characteristics and mechanisms of buildings in urban areas, the surface deformation monitoring data of three typical subdistricts were used as a reference. The horizontal and vertical deformations of the surface in the feature-1 area were relatively large; the maximum horizontal deformation and vertical settlement deformation were set to 14.4 mm/m and 13 mm/m, respectively. Feature-2 area was subjugated by vertical deformation of the ground surface; the horizontal deformation and vertical settlement were set to 4 mm/m and 10 mm/m, respectively. Feature-3 area was dominated by horizontal deformation of the ground surface, and its horizontal deformation and vertical settlement were set to 14.4 mm/m and 3 mm/m, respectively. In addition, the impact of mining-induced earthquakes on buildings in urban areas was also considered.

Analysis of Building Deterioration Characteristics

The calculation model of ABAQUS software and the form of the applied load are shown in **Figure 5**, and the length of the element was about 280 mm. The six-story masonry and frame building structures were considered for the analysis. To eliminate the calculation boundary effect and accurately reflect the coupling effect between the foundation and the building, the length, width, and depth of the lower stratum were taken as 37.9, 25.9, and 40 m, respectively. The horizontal and vertical deformation along the longitudinal direction of the building increased from zero to the maximum value in the subjected feature area. The mine seismic load was realized by applying the dynamic acceleration in the horizontal direction in the lower soil layer, as shown in **Figure 5D**. The time curve was selected from 1995 to 2003 after converting the maximum mine seismic level to the relevant data (Du, 2007).

The density, elastic modulus, and Poisson's ratio of the fourth soil layer were about 1860 kg/m^3, 400 MPa, and 0.2, respectively. The material of the structure and the foundation of the building were reinforced concrete, and the material properties of each component were shown in **Table 1**. The concrete damage plasticity model was used for the analysis, and the parameters of the model were considered in accordance with (Chengyuan, 2020) and they are not stated here.

Figure 6 shows the damage distribution of a masonry building affected by ground deformation action in each subjected region. Analysis showed that the masonry building in the feature-1 area was the most damaged, and the foundation part was almost completely damaged, and the damage to the bottom wall was also observed to be severe. Moreover, there were a few damaged areas existing at the top and bottom of the load-bearing columns in low level, while the damage to the non-bottom wall was relatively small, with only partial tilt-through cracks. This could also explain the dense and irregular distribution of reticulated cracks in the walls of the lower floors, the severe cracking and breakage of the bottom slabs of the balconies, and the severe penetration joints in the corners of the window and door openings of the buildings in this area. The damage to the foundation and walls of the building was relatively severe in the feature-2 area, as shown in **Figure 7**. Since the feature-3 area

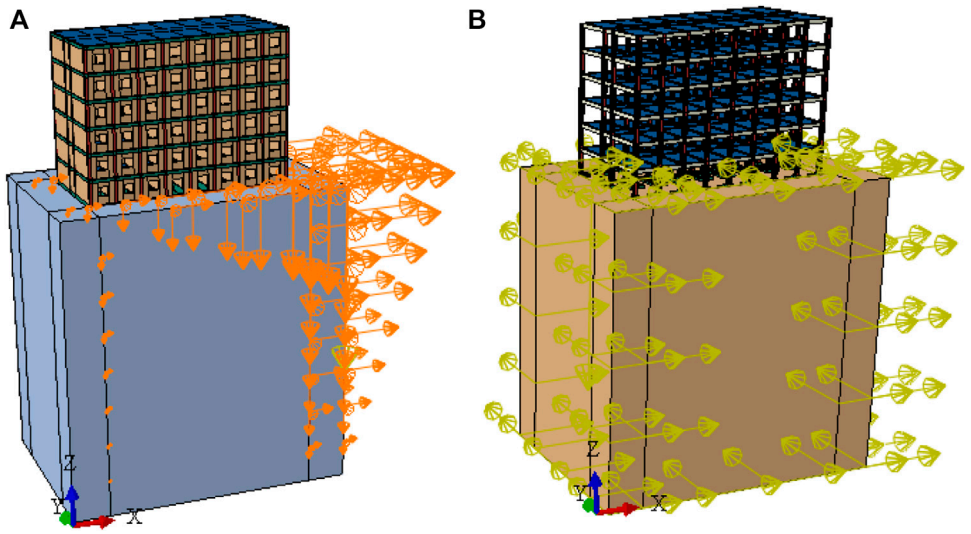

FIGURE 5 | Calculation model and load distribution: **(A)** ground deformation load applied to buildings; **(B)** buildings subjected to mine seismic loads.

TABLE 1 | Material properties of building components.

Components	Modulus of Elasticity/GPa	Poisson's Ratio	Density/kg·m^{-3}
Beams, foundations	30.340	0.2	2400
Column	31.530	0.2	2400
Floor	31.255	0.2	2400
Wall	30.340	0.2	2400

was under the influence of horizontal displacement of the ground surface, the foundation components were mainly damaged, and the upper wall had a low degree of damage. This can better explain the problem of cracking and detachment of superstructure and foundation of building in this area (**Figure 8**).

Figure 9 shows the damage distribution of frame structured buildings affected by ground deformation in each subjected area. Analysis showed that the framed buildings have better resistance to deformation than masonry buildings. By the superposition of horizontal and vertical displacement of the ground surface, the foundation part produced a small damage in a frame structure building. In addition, under the effect of uneven ground settlement, the structural columns of the ground floor and foundation components produced partial and large damage, respectively.

Figure 10 shows the damage distribution of the building under the coupled influence of mine quake and maximum ground deformation. The analysis showed that the damage to the walls of the masonry buildings was relatively serious, and the damage to main load-bearing elements, such as beams, slabs, and columns, was minor. The foundation was affected by the ground deformation and produced penetration damage. Masonry buildings with combined pile-raft foundations showed better resistance to deformation than buildings with raft foundations. The former significantly reduced the wall breakage on the ground floor of the building and showed a higher degree of damage in the upper walls.

Analysis of Reinforcement Scheme for Building Elements Under the Action of Slope Deformation

(1) Performance study of wall reinforcement material—steel fiber concrete

The results of both field research and numerical simulation of buildings in urban areas showed that buildings in each deformation feature area are damaged to a different extent. Repairing damaged parts of buildings in each region and enhancing resistance to deformation are prerequisites for improving the resilience of buildings against disasters. Therefore, to propose steel fiber reinforcement solutions for each characteristic deformation zone, the performance of various types of steel fiber concrete materials was simulated and calculated.

For this purpose, a 150 mm × 150 mm×150 mm standard specimen composed of C30 concrete and steel fiber of Q235 steel was used as an object for loading and force analysis. The range of steel fiber doping was 0.8%–1.5%, the range of steel fiber diameter was 0.6–0.9 mm, and the range of steel fiber length was 40–90 mm. The specifications of each group test are shown in **Table 1**. The length of steel fiber and concrete elements was 4.5 and 10 mm, respectively. The load applied to the specimen was divided into a uniform displacement of 10 mm and an inhomogeneous displacement standardized by the amount of

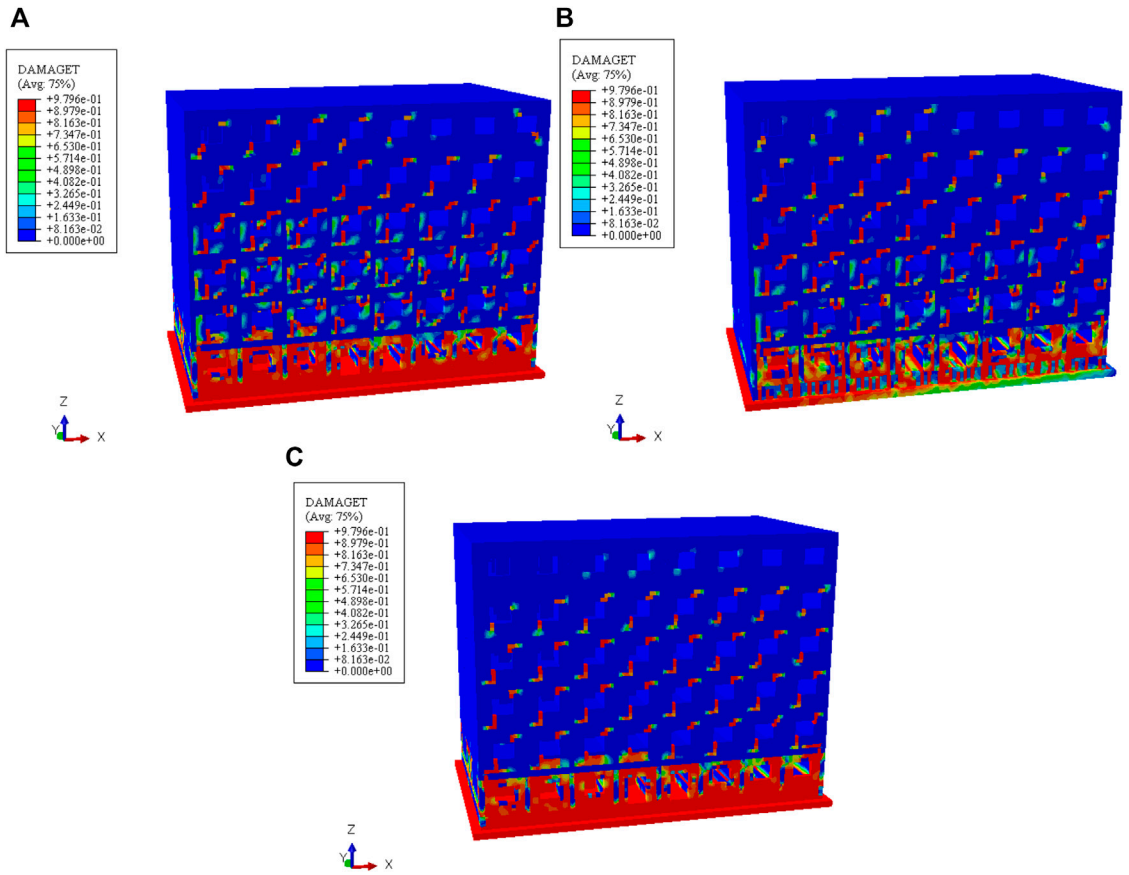

FIGURE 6 | Deformation damage distribution of masonry buildings in each deformation zone: **(A)** building damage under the effect of surface deformation in feature-1 area; **(B)** buildings damage under the effect of surface deformation in feature-2 area; **(C)** buildings damage under the effect of surface deformation in feature-3 area.

ground deformation in the three deformation feature areas, as per **Eqs 1–3**.

$$z_1 = -0.0274 \times (x - 75) \quad (1)$$

$$z_2 = -0.0141 \times (x - 75) \quad (2)$$

$$z_3 = -0.0174 \times (x - 75) \quad (3)$$

Figure 11 shows a simulated specimen block of steel fiber concrete with internal fibers depicted by randomly generated line segments, thus coinciding with the actual preparation test process. The deformation resistance of concrete specimens of each mixing scheme (Groups 1–6 in **Table 2**) was analyzed under different loads, and the calculated results are shown in **Figure 12**.

The analysis showed that concrete with 0.8% steel fiber has a 10% higher resistance to deformation under uniform tensile load than standard concrete. However, a small increase in the deformation resistance of concrete specimens was observed with the increase in the amount of steel fiber admixture beyond 0.8%. It was observed that under relatively large non-homogeneous loads representative of the effect of maximum deformation of the ground surface in the feature-1 area (**Figure 12B**), the steel fiber concrete showed an almost 100% increase in the deformation resistance as compared to standard concrete. In addition, an increase in the length of the steel fiber was also observed to strengthen the deformation resistance of the concrete. Under relatively small non-homogeneous loads representative of the effect of surface displacement deformation in the feature-2 area, there was a small increase of up to 10% in the deformation resistance by steel fiber concrete compared to the standard concrete. Therefore, steel fiber concrete is more suitable for strengthening the more vulnerable parts of the buildings in the feature-1 area that show cracking and other tensile damages; less vulnerable parts of the buildings, both plain concrete and steel fiber concrete, are of similar suitability.

(2) Analysis of deformation resistance of Concrete columns and Beams

① Analysis of deformation-resistant reinforcement of concrete columns

Improving the deformation resistance of structural columns can effectively reduce the overall damage and cracking of the

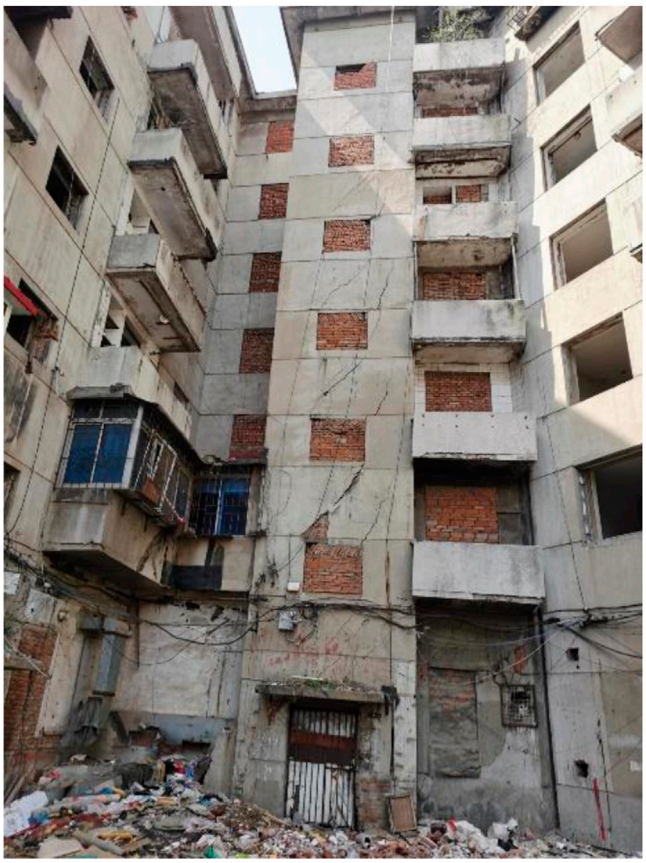

FIGURE 7 | Cracking of building wall and damage of balcony in feature-2 area.

buildings since they are the main load-bearing components of the buildings. For the deformation characteristics and forms of urban ground, the reinforcement methods of carbon-fiber-reinforced polymer (CFRP)-reinforced concrete columns and carbon-fiber-board-covered concrete columns are proposed.

Analysis showed that the CFRP-reinforced concrete columns had better-sustained resistance to deformation than ordinary concrete columns, and the concrete columns had better resistance to deformation even after partial damage, and CFRP-reinforced concrete columns had high peak stresses. As shown in **Figure 13B**, CFRP concrete reinforced columns and CFRP wrapped concrete columns had better resistance to deformation in each area of ground deformation, which is especially suitable for reinforcement of building elements with a large degree of deformation. The specific indexes and data of the deformation resistance of the three types of concrete columns under the influence of side slope deformation are shown in **Table 3**.

Figure 14 shows the damage distribution of CFRP-wrapped concrete reinforced columns, CFRP reinforced concrete columns, and plain concrete columns subjected to uneven loading. For the simulation, the site condition of the building in the urban area was used as a reference; the cross-sectional width and height of the concrete square column were 380 and 2800 mm, respectively, and the type of concrete was C30. The CFRP-wrapped concrete reinforced columns were reinforced using 25 mm thick CFRP plates wrapped around the concrete columns, and the CFRP reinforced concrete columns were reinforced using 16 mm CFRP columns arranged at 50 mm intervals.

The analysis of the damage distribution state of the three types of concrete columns under the uneven ultimate load showed that the damage of the CFRP-reinforced concrete columns and the CFRP-wrapped concrete columns was minor compared to the ordinary concrete columns. The upper part of the ordinary concrete column was almost completely broken. It is feasible to strengthen the concrete columns of existing buildings with CRFP slabs, and build CFRP columns reinforced load-bearing concrete columns.

② Analysis of deformation resistance of concrete beams

The beams are the central part of the building structure to bear the force deformation and are easy to break; using a CRFP plate for its reinforcement can effectively improve the overall deformation resistance performance. A concrete beam with a span of 5,900 mm and a cross-sectional height and width of 380 and 370 mm, respectively, was used to compute and analyze the deformation resistance with and without CFRP slab reinforcement. The simulation results are shown in **Figure 15**.

The degree of damage in the middle and lower regions was significantly reduced as the CFRP wrapped concrete beam was used, and no concrete dislodgement was observed, and the CFRP-wrapped concrete beam had partial load-carrying capacity. However, the small concrete peeling area on the upper surface of both ends of the beam can be repaired by steel fiber concrete filling. The degree of damage to ordinary concrete beams was relative of severe nature, and concrete dislodging was observed in the middle, corner, and lower parts. Consequently, the overall resistance to deformation of the ordinary concrete was significantly low.

FIGURE 8 | Separation of building a wall from the foundation in feature-3 area.

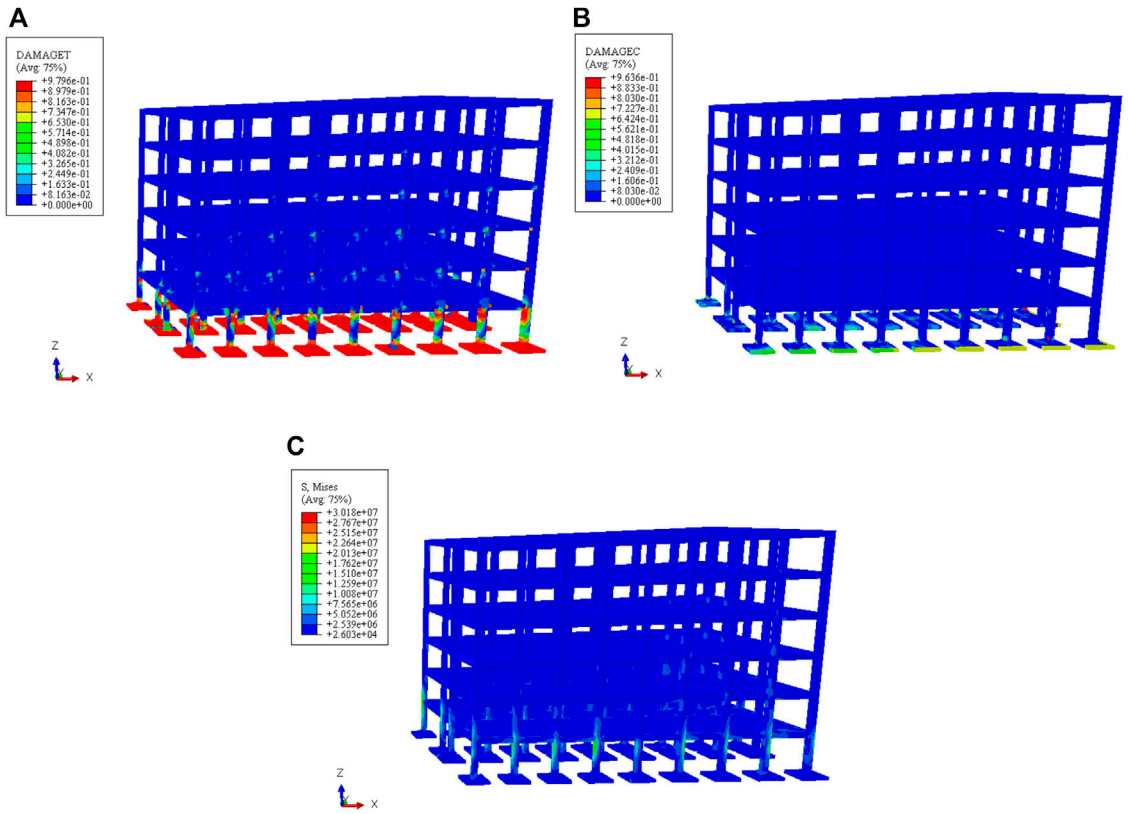

FIGURE 9 | Distribution of deformation and damage of frame structures in each deformation area: **(A)** buildings damage under the effect of surface deformation in feature-1 area; **(B)** buildings damage under the effect of surface deformation in feature-2 area; **(C)** buildings damage under the effect of surface deformation in feature-3 area.

(3) Study on flexural performance of reinforced Concrete slabs wrapped with profile steel

The floor slab of the building was more severely damaged due to the uneven settlement caused by the ground deformations. It was hypothesized that by wrapping the concrete slab with C and E-shaped steel plates, the deformation resistance of the concrete slab could be improved. The compressive bending deformation of an ordinary and shaped steel plates strengthened of the concrete slab was considered for analysis, and the length width and thickness of the concrete slab were taken as 100 mm, 45 mm, and 8 mm, respectively. Moreover, the applied displacement deformation was taken as 10% of the thickness, and the types of concrete and steel were set to C30 and Q235R, respectively.

The plastic deformation under the load was selected as the evaluation index of the deformation resistance of the concrete slab. As shown in **Figure 16**, the plastic deformation of the C-shaped steel-wrapped concrete slab was only one-third of that of ordinary concrete. Thus, the bottom and top floor slabs of buildings in urban areas with serious damage could be strengthened by steel sections to improve stability.

Toughness Enhancement Scheme of Buildings Against Slope Deformation

(1) Building foundation and wall reinforcement

Some buildings in feature-1, feature-2, and feature-3 areas were affected by side slope deformation and ground cracks and showed serious wall cracking, external bulging, and shear damage to the foundation. Based on the analysis results in this study, it was recommended that pertinent parts of buildings be reinforced with steel fiber concrete to mitigate and repair the aforementioned damages.

(2) Building wall column and Balcony reinforcement

The wall column and balcony reinforcement areas were severely damaged in the northern (feature-1 and feature-2 areas) and the south bank, and there existed many vulnerable buildings in these areas construction of which was more than 30 years old. The buildings in these regions were subjected to uneven ground settlement deformation forces, resulting in wall cracking, wall misalignment, damage to wall-column joints, and balcony breakage. This damage could be reinforced with CRFP wrapped concrete columns, balcony slabs, etc.

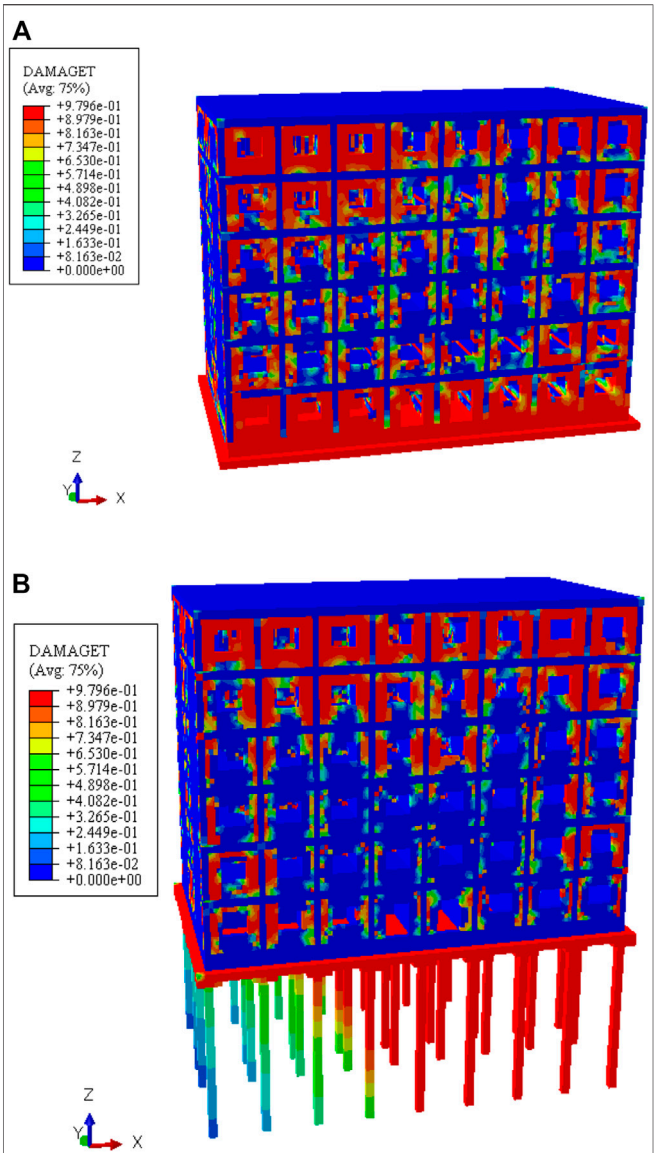

FIGURE 10 | Distribution of deformation and damage of masonry buildings with different foundation forms: **(A)** masonry buildings with raft foundations; **(B)** masonry buildings with combined pile-raft foundations.

(3) Beam and floor slab reinforcement

In the area close to the slope of the mine, the ground surface was prone to be affected by the slope deformation thus could have a large horizontal ground surface deformation. Multi-story masonry structure buildings in these areas experienced beam damage, floor deflection and other pertinent phenomena. As per the findings of this study, to mitigate and repair the beam-and floor-related damages, external CFRP wrapping of beam and reinforcement of slab with steel section could be employed, respectively. Moreover, the steel fiber concrete filler could be used to strengthen the concrete shedding areas in these parts of buildings. Similarly, buildings with different deterioration characteristics could be reinforced with different measures, as shown in **Table 4**.

DISASTER PREVENTION AND EMERGENCY RESILIENCE ENHANCEMENT IN URBAN AREAS AROUND SLOPES

A comprehensive and multifaceted approach to disaster resilience enhancement based on the criteria of disaster resilience grading zones in urban areas was established to improve the ability of geological disaster prevention and emergency response in the urban areas around the Fushun West Open-pit mine. This approach was aimed to protect the lives and properties of residents of this region and provide a scientific basis for the rational planning and construction of the to-be-built communities.

Urban Disaster Prevention and Emergency Zoning

Figure 17 shows the zoning of the emergency geohazard protection level in the urban area around the west open pit of Fushun City; the zoning was based on the field monitoring of displacement, the population density of the cluster, the stratigraphic stability conditions, and the landslide history of the slopes. The protection levels were set as levels one, two, and three, wherein the required care increased from high to low. The residential areas in the south of Nan'yang Road, on the northeast bank, on the south bank of Qian-tai mountain, in the mine area were the key areas with high population density marked as to require level 1 protection (shown by the red region in **Figure 17**). The northern area of Nan'yang Road in the northern bank, the Dong'li and the Wu'lao community area in the southern bank, were classified to require level 2 protection (shown by the orange region in **Figure 17**). The low population concentration areas, including the industrial park on the north bank, the industrial park on the southwest bank, and the industrial park on the south bank, were jointly designated as level 3 protection regions (shown by the green region in **Figure 17**).

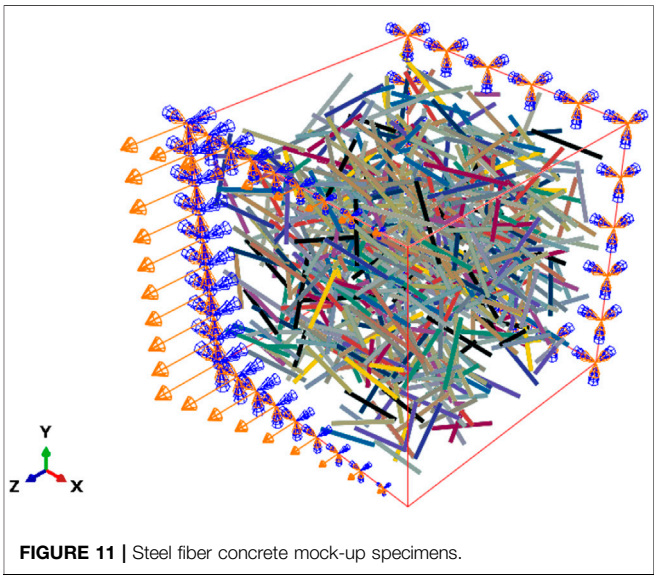

FIGURE 11 | Steel fiber concrete mock-up specimens.

TABLE 2 | Fiber mixing scheme for each group of test blocks.

Number	Fiber Dose (%)	Fiber Diameter (mm)	Fiber Length Range	Number of Fibers
Group one	0.8	0.8	60–90 mm	716
Group two	1.0	0.6	50–70 mm	1989
Group three	1.0	0.9	55–95 mm	707
Group four	0.8	0.9	85–95 mm	472
Group five	1.2	0.7	50~-90 mm	1503
Group six	1.2	0.6	45–75 mm	2387
Group seven	1.5	0.7	80–100 mm	1461
Group eight	1.5	0.8	40–80 mm	1679

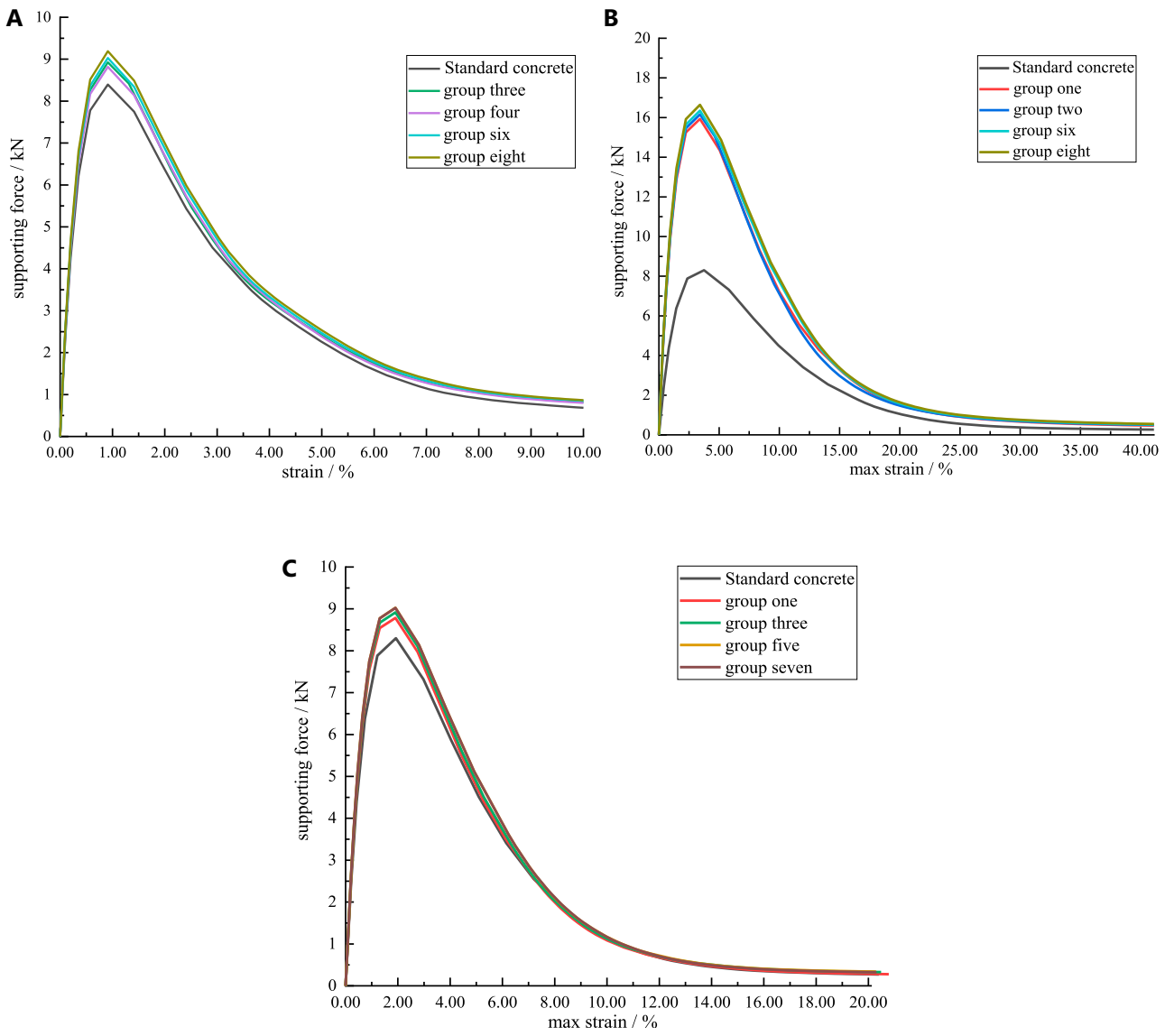

FIGURE 12 | Comparison of deformation resistance curves of steel fiber concrete specimens and standard specimens: **(A)** support force and strain curve of test block under uniform tension; **(B)** support force versus strain curves of test blocks under equivalent non-uniform tension in the feature-1 area; **(C)** support force versus strain curves of test blocks under equivalent non-uniform tension in feature-2 area.

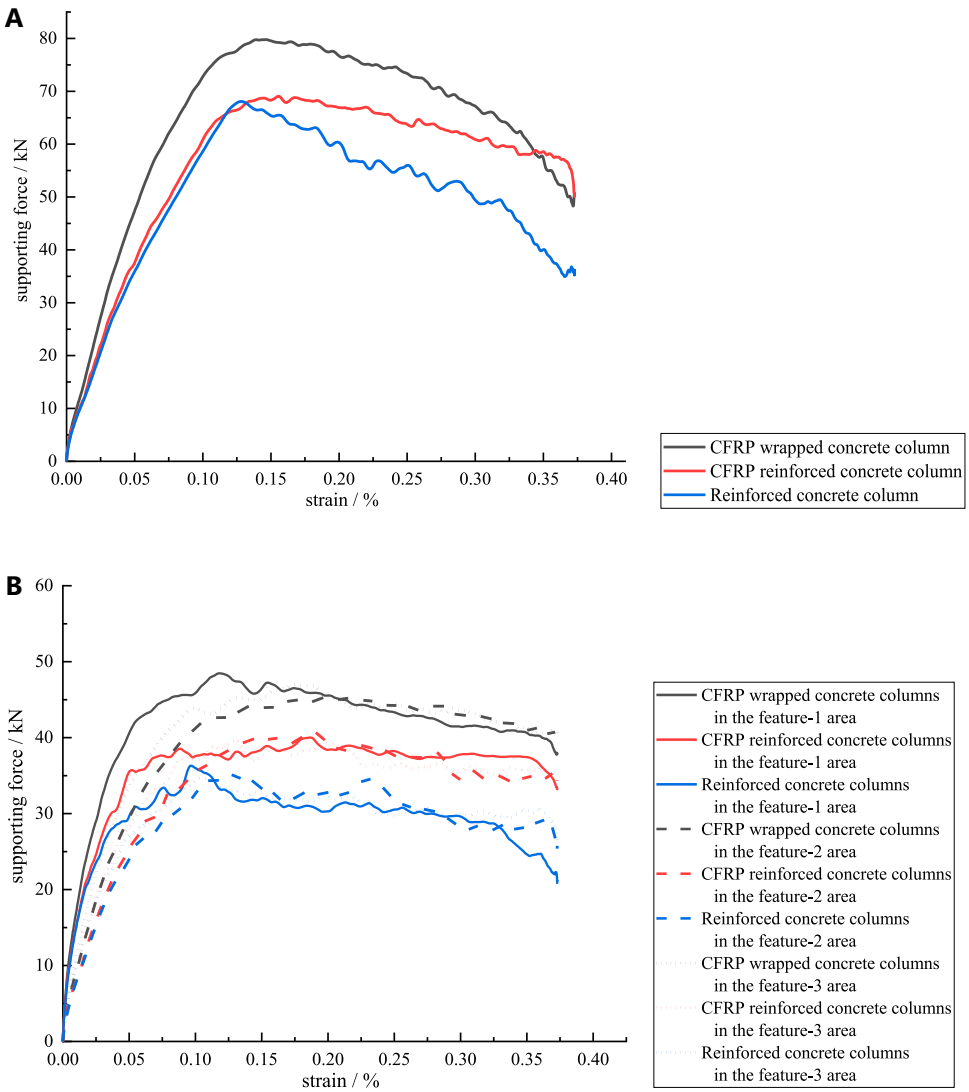

FIGURE 13 | Analysis of deformation resistance of CFRP concrete reinforced columns: **(A)** support force and strain curves of concrete columns under uniform load; **(B)** support force and strain curves of concrete columns under loads in each characteristic zone.

TABLE 3 | Deformation resistance of each type of column.

Column types	Resistance to Uniform Deformation		Resistance to Uneven Deformation	
	Ultimate Bearing Capacity (kN)	Post-peak Load-Bearing Capacity (kN)	Ultimate Bearing Capacity (kN)	Post-peak Load-Bearing Capacity (kN)
reinforced concrete columns	79776.9	63336.1	48472.6	42031.7
			45302.8	42163.6
			46997.0	42436.3
CFRP concrete reinforced columns	69088.3	59984.3	40012.0	36618.8
			40682.5	35872.5
			39661.1	36061.9
CFRP wrapped concrete columns	68071.8	48039.0	36306.1	27851.8
			35221.6	29730.9
			34743.1	30340.4

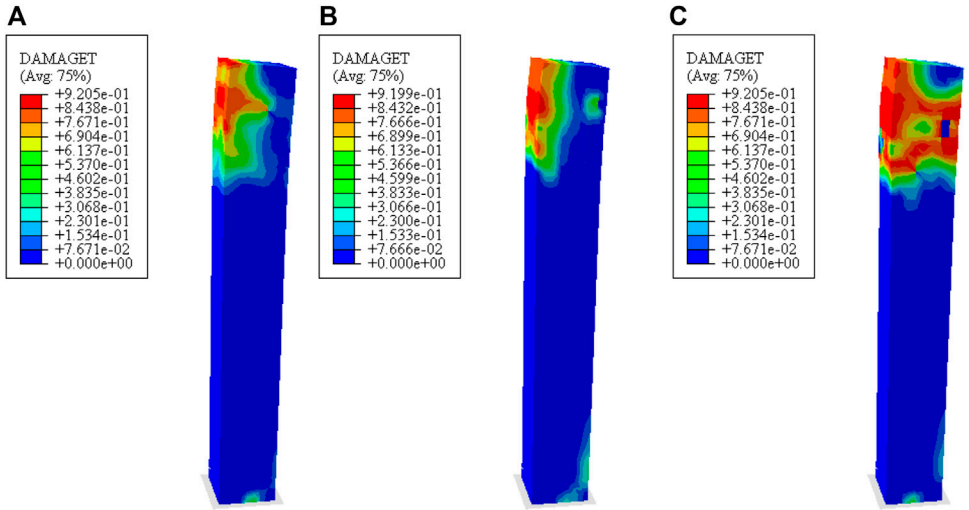

FIGURE 14 | Breakage of various types of concrete columns under equivalent ultimate load in feature-1 zone: **(A)** CFRP-wrapped concrete reinforced columns; **(B)** CFRP reinforced concrete columns; **(C)** ordinary reinforced concrete columns.

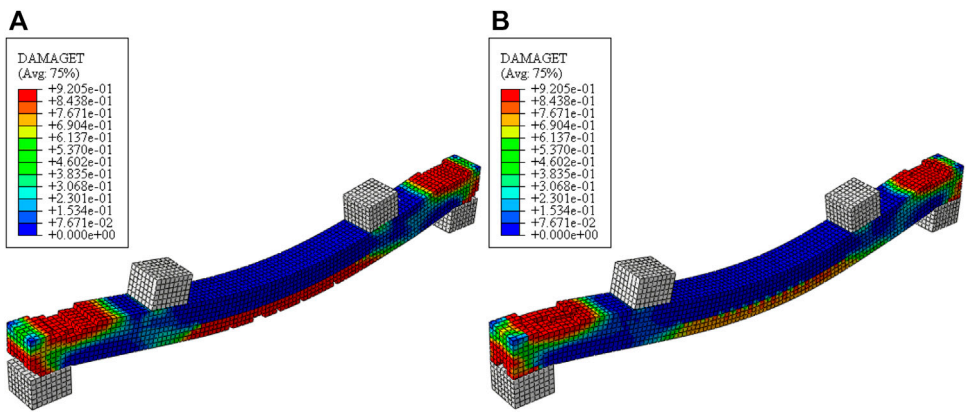

FIGURE 15 | Concrete beams under load damage: **(A)** ordinary reinforced concrete beams; **(B)** CFRP wrapped concrete reinforced beams.

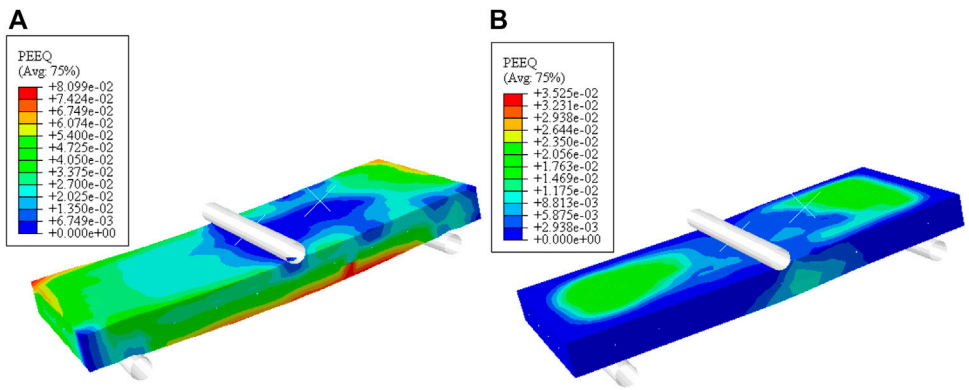

FIGURE 16 | Plastic deformation of concrete slabs under load: **(A)** plastic deformation of the reinforced concrete slab; **(B)** plastic deformation of C-shaped steel wrapped concrete slab.

TABLE 4 | Causes of damage to building elements and reinforcement measures in each region.

Type of Damage	Causes of Damage	Reinforcement Measures	Scope of Application (Type of Building and Number of Floors)
Wall cracking	Uneven settlement of foundation; unreasonable building construction, poor integrity of old and new walls	Steel fiber concrete repair and reinforcement	Masonry and frame buildings with more than five floors
Wall misalignment	Horizontal deformation of the ground surface		
Beam cracking	Ground deformation, insufficient stiffness	CFRP concrete reinforcement	Masonry and frame buildings with more than five floors
Column tilt and cracking	Uneven ground settlement, insufficient stiffness	Overmolded steel reinforcement	Masonry buildings of five floors and below
Base plate cracking		CFRP concrete reinforcement	Masonry and frame buildings with more than five floors
Balcony breakage	Ground deformation, construction causes	Balcony bracing method reinforcement, CFRP concrete reinforcement	Masonry buildings of five floors and below
Basic detachment	Uneven foundation settlement, insufficient foundation stiffness or excessive foundation stiffness	High toughness and high strength concrete reinforcement	Masonry structure

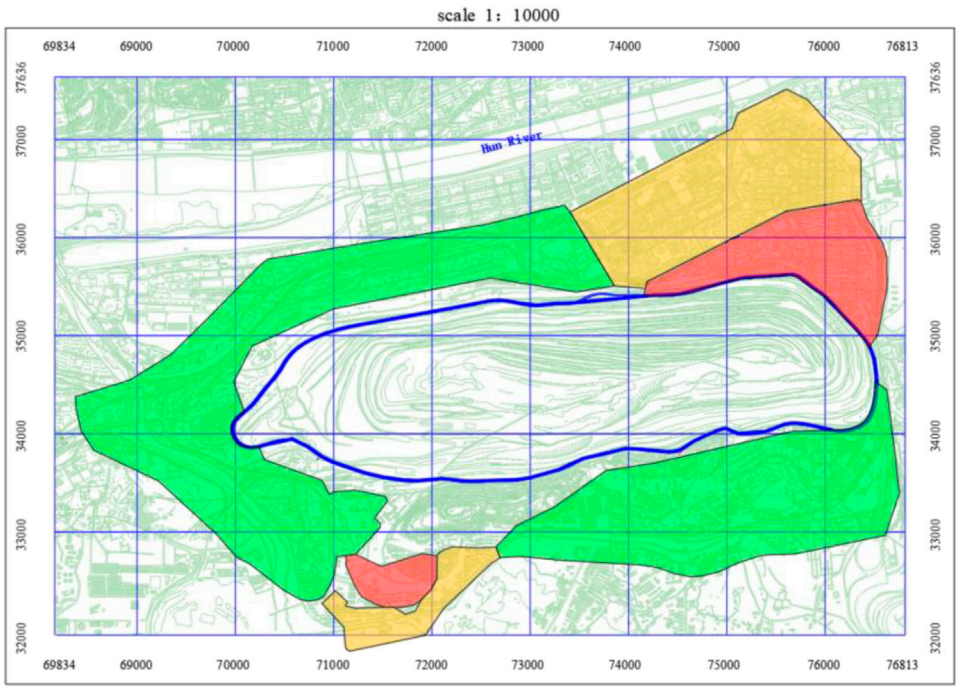

FIGURE 17 | Emergency fortification zoning of slope disasters in the affected area.

Disaster Preparedness Resilience Enhancement Methods for Established Communities

The resilience enhancement approach for established communities needs to consider community resilience enhancement strategies in terms of redundancy, efficiency, and adaptability. The strategies are established based on three major aspects, i.e., engineering, organization, and system.

From the perspective of engineering, concrete or mortar filling, and reinforcement are recommended to be employed on the exterior walls, columns, and balconies of existing buildings (structures) in the community. The foundations of buildings in areas with large surface displacement variables are recommended to be repaired and reinforced. Permanent or temporary shelters are recommended to be established according to the population density and age structure of people in the community, and necessary emergency signs should be set up.

In terms of organization, a set of organizational structure systems is recommended to be established by making the community neighborhood committee a governing body. The contacts of the community with the municipal emergency management bureau, fire rescue teams, and other

departments are recommended to be strengthened to achieve timely and effective information sharing and rescuing. The community should be scientifically zoned to establish multiple responsibility areas with dedicated staff responsible for managing day-to-day disaster prevention and mitigation matters, especially in special circumstances, i.e., the rainy season. The necessary emergency devices should be used, and emergency access should be set up to improve the efficiency of community disaster prevention and emergency response. Moreover, disaster prevention and mitigation education and drills should be conducted for the communities.

From the perspective of system construction, the establishment and implementation of disaster detection prevention and reporting systems are recommended.

Disaster Resilience Enhancement Methods for Unbuilt Communities

For unbuilt and to-be-built communities, technical feasibility and economic applicability are the principles according to national norms and geological characteristics of the urban areas. The three proposed resilience enhancement methods and strategies are as follows.

(1) New communities should be sited as far away from the west open pit as possible, avoiding adverse geological area such as faults and fractures.
(2) The deformation of the ground surface of the characteristic area and geological emergency defense level must be considered. The foundation type and building structure with a better bearing capacity of regional surface deformation should be chosen. Reasonable design of building elements such as settlement joints, expansion joints and flexible bearings can absorb part of the building deformation, thus improving the deformation resistance of community buildings.
(3) A reasonable disaster-proof space and a sound management system should be designed and built. This implies that we should improve infrastructure construction, increase medical services, plan community-specific disaster prevention land, and increase the area of public open space. In the primary prevention area, the new community should develop a complete emergency and disaster prevention plan for geological hazards and engage professional staff to monitor and warn about the hidden hazards throughout the year. In the secondary prevention area, new communities should formulate emergency and disaster prevention plans for geological hazards and strengthen the inspection of potential disaster sites during the rainy seasons and freezing and thawing periods.

CONCLUSION

(1) The slope deformation of the west open pit and the surrounding urban areas from 2016 to 2020 is slow, and there are roughly three areas of relatively large surface deformation within the pit. There are roughly three areas with relatively large surface deformation in the pit, namely, the western drainage field, the south bank of slope area (former landslide body area), and the eastern area of the north bank.
(2) The surface of the surrounding urban area is mainly affected by slope creep deformation, ground fracture. According to the different magnitudes of horizontal and vertical deformations of the ground surface, the northern bank, the eastern part of the northern bank, the central part in the northern bank, and the area of Qian-tai mountain in the south can be divided into three deformation featured partitions. The deformation in the area of petroleum plant No.1 is a coupled horizontal and vertical ground surface deformations, the vertical ground surface deformation is dominant in the area affected by the fracture in the middle of the north bank, and the horizontal deformation is dominant in the Qian-tai mountain area.
(3) Frame structure has better resistance to side slope deformation than masonry structure, and the buildings of both types of structural forms have a pronounced damage under the coupled action of the horizontal and vertical side slope deformations. The foundation part of the building of the masonry structure is affected by the horizontal deformation to a higher degree, and the upper wall is affected by the uneven settlement, while the foundation of the frame structure is affected by vertical deformation of the slope.
(4) Steel fiber concrete reinforced walls, CFRP concrete reinforced beams and columns, and section steel reinforced floor slabs are proposed methods to enhance the deformation resistance and resilience of buildings in urban areas. All these methods can effectively improve the ability of buildings in urban areas to resist side slope deformation.
(5) A three-level urban geological disaster prevention and emergency treatment zone map is established based on the side slope deformation, population density and the degree of building damage in each feature area of the urban region, and the resilience enhancement methods for the built and to-be-built communities are also established.

DATA AVAILABILITY STATEMENT

The original contributions presented in the study are included in the article/supplementary material, further inquiries can be directed to the corresponding author.

AUTHOR CONTRIBUTIONS

The first author,ZJ, is responsible for the general writing of the full text and completing the main work; the second author,LF, and the third author, WJ, are responsible for gatekeeping; the fourth author, GA, and the fifth author,HC, are responsible for consulting on a small number of issues.

FUNDING

We acknowledge the funding support from the National Key Research and Development Project of China (Grant No. 2017YFC1503104).

REFERENCES

Chen, H., Li, G., Fang, R., and Zheng, M. (2021). Early Warning Indicators of Landslides Based on Deep Displacements: Applications on Jinping Landslide and Wendong Landslide, China[J]. *Front. Earth Sci.* 9. doi:10.3389/feart.2021.747379

Chen, Z., Fang, C., and Deng, R. (2015). "Research and Application of Jinggangshan Geological Disaster Prevention System Based on Wireless Sensor Network System[J]," in 2015 23rd International Conference on Geoinformatics (Wuhan, China: IEEE), 1–5.

Chengyuan, H. E. (2020). *Research on Damage Analysis and Deformation Control of Buildings in the Influence Area of Fushun West Open-Pit Mine [D]*. Beijing: University of Science and Technology. (In Chinese).

Du, D. (2007). *Research on Mining-Induced Seismicity in Fushun Laohutai Coal Mine and its Effect on Building [D]*. Liaoning: Liaoning Technical University. (In Chinese).

Du, Y., Xie, M., Jiang, Y., Huo, L., Chen, C., Jia, B., et al. (2021). Review on the Formation Mechanism and Early Warning of Rock Collapse[J]. *Metal. Mine* 535 (01), 106–119. (In Chinese). doi:10.19614/j.cnki.jsks.202101008

Du, Y., Xie, M., and Jia, J. (2020). Stepped Settlement: A Possible Mechanism for Translational Landslides. *CATENA* 187, 104365. doi:10.1016/j.catena.2019.104365

Gao, A. (2020). *Study on Damaged Location Characteristics and Anti-deformation Methods of Buildings in Affected Area of Fushun Western Open-Pit Mine[D]*. Beijing: University of Science and Technology. (In Chinese).

Gao, A., Wang, J., Li, F., and Xie, J. (2021). Locational Characteristics of Damage on Buildings Around the West Open-Pit Mine[J]. *Meitan Xuebao/Journal China Coal Soc.* 46 (4), 1320–1330. (In Chinese).

Gulec, A., Kose, M. M., and Gogus, M. T. (2021). Experimental Investigation of Flexural Performance of T-Section Prefabricated Cage Reinforced Beams with Self-Compacting Concrete. *Structures* 33 (5), 2190–2197. doi:10.1016/j.istruc.2021.05.074

He, F., Tan, S., and Liu, H. (2022). Mechanism of Rainfall Induced Landslides in Yunnan Province Using Multi-Scale Spatiotemporal Analysis and Remote Sensing Interpretation. *Microprocess. Microsystems* 90, 104502. doi:10.1016/j.micpro.2022.104502

La, R., Lv, T., Bai, P., and Zhang, Z. (2021). Research on Collaborative and Optimal Deployment and Decision Making Among Major Geological Disaster Rescue Subjects[J]. *Geotechnical Geol. Eng.* 1, 1–13.

Mostafa, K., Rahmat, M., Carlos, C., Mohammad Reza, E., and Luc, C. (2021). Numerical Study on the Flexural Behaviour of Normal- and High-Strength Concrete Beams Reinforced with GFRP Bar, Using Different Amounts of Transverse Reinforcement[J]. *Structures* 34, 3113–3124.

Ou, P., Wu, W., Qin, Y., Zhou, X., Huangfu, W., Zhang, Y., et al. (2021). Assessment of Landslide Hazard in Jiangxi Using Geo-Information Technology. *Front. Earth Sci.* 9, 648342. doi:10.3389/feart.2021.648342

Qiao, J., Liu, B., Li, Y., Li, S., and Zhang, W. (2022). Experimental Study on Shear Performance of Improved High-Performance Polymer Cement Mortar-Glass Fiber Reinforced Plastic Reinforced Masonry Wall. *Adv. Struct. Eng.* 25 (2), 247–258. doi:10.1177/13694332211046347

Resan, S. F., Zemam, S. K., and Abed, M. S. (2020). Developing Tension Field Action of Embedded Steel Plates-Stiffened Rebars Composite Reinforcement within Concrete Deep Beams[J]. *Adv. Struct. Eng.* 23 (7), 1710141054. doi:10.1177/1369433220919065

Rf, A., Rui, M. A., Apr, B., and Cj, A. (2020). Influence of the Top Reinforcement Detailing in the Behaviour of Flat Slabs[J]. *Structures* 23, 718–730.

Shao, L. (2019). Geological Disaster Prevention and Control and Resource Protection in Mineral Resource Exploitation Region[J]. *Int. J. low carbon Technol.* 14, 142–146. doi:10.1093/ijlct/ctz003

Tsai, W. N., Chen, C. C., Chiang, C. W., Chen, P. Y., Kuo, C. Y., Wang, K. L., et al. (2021). Electrical Resistivity Tomography (ERT) Monitoring for Landslides: Case Study in the Lantai Area, Yilan Taiping Mountain, Northeast Taiwan[J]. *Front. Earth Sci.* 9, 1. doi:10.3389/feart.2021.737271

Xu, Y., Qiu, X., Yang, X., Lu, X., and Chen, G. (2020). Disaster Risk Management Models for Rural Relocation Communities of Mountainous Southwestern China under the Stress of Geological Disasters. *Int. J. Disaster Risk Reduct.* 50, 101697. doi:10.1016/j.ijdrr.2020.101697

Conflict of Interest: Author GA was employed by the company Shanxi Academy of Building Research Co., Ltd. Author HC was employed by the company China Railway Bridge Research Institute, Ltd.

The remaining authors declare that the research was conducted in the absence of any commercial or financial relationships that could be construed as a potential conflict of interest.